Probabilistically-Safe Bipedal Navigation over Uncertain Terrain via Conformal Prediction and Contraction Analysis

***Abstract*— We address the challenge of enabling bipedal robots to traverse rough terrain by developing probabilistically safe planning and control strategies that ensure dynamic feasibility and centroidal robustness under terrain uncertainty. Specifically, we propose a high-level Model Predictive Control (MPC) navigation framework for a bipedal robot with a specified confidence level of safety that (i) enables safe traversal toward a desired goal location across a terrain map with uncertain elevations, and (ii) formally incorporates uncertainty bounds into the centroidal dynamics of locomotion control. To model the rough terrain, we employ Gaussian Process (GP) regression to estimate elevation maps and leverage Conformal Prediction (CP) to construct calibrated confidence intervals that capture the true terrain elevation. Building on this, we formulate contraction-based reachable tubes that explicitly account for terrain uncertainty, ensuring state convergence and tube invariance. In addition, we introduce a contraction-based flywheel torque control law for the reduced-order Linear Inverted Pendulum Model (LIPM), which stabilizes the angular momentum about the center-of-mass (CoM). This formulation provides both probabilistic safety and goal reachability guarantees. For a given confidence level, we establish the forward invariance of the proposed torque control law by demonstrating exponential stabilization of the actual CoM phase-space trajectory and the desired trajectory prescribed by the high-level planner. Finally, we evaluate the effectiveness of our planning framework through physics-based simulations of the Digit bipedal robot in MuJoCo.**

I. Introduction

Bipedal locomotion holds great promise for navigating unstructured and challenging environments, as they can adapt to irregular terrain through discrete and precisely controlled footstep placement [1], [2]. However, locomotion over uncertain terrain remains susceptible to instability, particularly when consecutive footsteps must be placed on surfaces with significant geometric variability and centroidal momentum needs to be regulated accurately. Many biped navigation frameworks [3]–[5] address terrain uncertainty at the high-level planning but omit corrective motion strategies in low-level control with confidence-guaranteed on the uncertainty. To address this challenge, we develop a terrain-uncertainty-aware planning and control framework that formally quantifies terrain elevation uncertainty and leverages it to achieve provably-safe footstep planning with a specified probability threshold, while guaranteeing forward invariance of the centroidal states in a robust tube around the desired motion plan. Such a framework ensures locomotion balance and supports the generation of probabilistically-safe and dynamically-feasible locomotion plans over long horizons (see Fig. 1).

In our bipedal robot navigation framework, we leverage a reduced-order robot model, i.e., the Linear Inverted Pendulum Model (LIPM), to design a high-level planner for

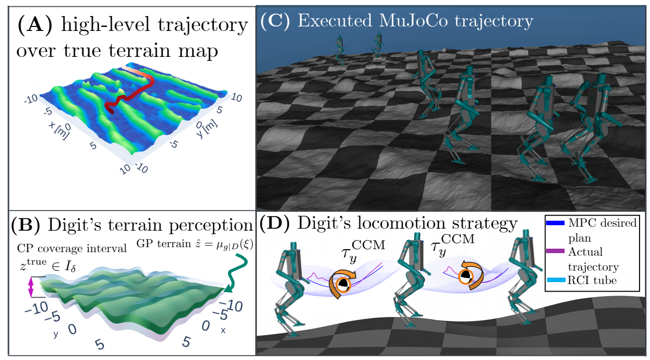

Fig. 1. (A) A bird's-eye view of the robot navigation path over the true rough terrain map. (B) A visualization of terrain map estimated by Gaussian Process (GP) and conformal prediction (CP). (C) The bipedal robot Digit navigates through an environment with rough terrain in our MuJoCo simulation. (D) Digit's flywheel torque control law maintains the CoM trajectory within the contraction-based robust control invariant tube on the robot with full-order dynamics.

the center-of-mass (CoM) and footstep plans under a user-specified probability of safety. In particular, we derive uncertainty bounds on the LIPM-based robot dynamics caused by the terrain using conformal prediction (CP). Then, we use the derived uncertainty bounds to construct contraction-based reachable tubes around the nominal plans given by the high-level planner, while, at the low-level, a flywheel torque controller is designed to stabilize centroidal angular momentum induced by terrain variations. The integration of both uncertainty-aware CoM planning and the corrective torque controller guarantees dynamic safety under a user-defined probability, and the motion plans executed online are guaranteed to remain in a compact forward invariant set around the desired CoM motion plan. The key contributions and organization of this work are as follows:

- We adopt a Gaussian process (GP) regression model with an Attentive Kernel (AK) for mapping nonstationary terrain. We then couple the GP model with CP to construct data-calibrated confidence intervals, ensuring high-confidence coverage of the true terrain elevations.
- We propose an uncertainty-informed model-predictive-control (MPC) framework for bipedal navigation over rough terrain. Given a predefined high probability of safety, the MPC guarantees provably-safe CoM planning toward a desired goal, up to a specified probability, via CP-informed footstep sequence selections and minimization of traversal terrain slopes.
- To reliably track MPC plans, we derive a contraction-based flywheel torque control law for correcting off-nominal centroidal angular momentum caused by terrain perturbations. We use contraction theory and the

CP bounds to compute time-varying reachable tubes, guaranteeing forward invariance and exponentially-stabilizing behavior toward the desired trajectory.
- Finally, we discuss the gap of our contraction analysis relative to the full-order robot dynamics and demonstrate the validity of our planning and control strategy on a Mujoco simulation of the Digit robot.

II. Related Work

A. Bipedal Locomotion over Rough and Uncertain Terrain

Long-horizon bipedal planning over irregular, uncertain terrain has been widely studied [2]–[5]. [2] uses piecewise-linear terrain approximation and friction cone constraints for foot placement but requires prior terrain knowledge and ignores uncertainty. [5] proposes a terrain-aware MPC penalizing slope for stable locomotion but uses uncertainty only in a traversability score for high-level navigation. [3] combines a Control-Lyapunov-Function controller with a sampling-based planner and traversability metrics to avoid high-cost regions, while [4] learns terrain online via a GP but conservatively bypasses uncertain areas. Both methods limit robots to a limited set of paths, whereas our work enables traversing broader uncertain regions with probabilistic safety guarantees.

B. Reduced-order Locomotion Planning and Control

In online optimal control for humanoid centroidal balancing, reduced-order models (ROMs) such as the LIPM [6], [7] are widely used to maintain tractability and predict centroidal motion. These models integrate with step-adaptation and momentum regulation to stabilize dynamic locomotion under mismatch between ROM-based planning and full-body control [8]. [9] enables non-periodic CoM trajectories and 3D footstep planning on uneven terrain with dynamic programming for flywheel torque. The angular momentum LIP (ALIP) model [2] applies MPC-based footstep planning over uneven terrain. However, most of these works lack uncertainty quantification and formal safety guarantees. We instead leverage ALIP with flywheel torque control and contraction analysis to design a robust controller guaranteeing high-probability tracking of full-order dynamics.

C. Contraction Theory

Control contraction theory [10] provides a unified framework for nonlinear control with formal robustness and convergence guarantees. Contraction-based controllers for control-affine systems [11] enable incremental stabilizability and have been applied to compute tracking tubes under disturbances in robotics [12]. [12] designs uniform upper-bound ellipsoids around trajectories given disturbance bounds, while [13] proposes spatially varying bounds reflecting learned dynamics. Most work applies contraction-based tubes to high-level planning, with limited focus on phase-portrait analysis for low-level motion feasibility. We introduce the first contraction-based controller for locomotion phase portraits, reducing discrepancies between ROM references and full-order dynamics to enable robust tracking under model and environmental uncertainties.

D. Conformal Prediction

Conformal prediction (CP) provides statistically rigorous prediction intervals with guaranteed coverage independent of model or data [14], [15]. For robotic planning, [16] applies CP to neural-network path predictions, ensuring collision-free paths at a set probability. [17] derives disturbance bounds from the GP posterior for contraction analysis, but limited data can yield overly conservative bounds, and kernel assumptions may underestimate model error. [18] instead advocates CP-refined GP intervals. Building on this, we use CP to tighten GP bounds and calibrate them directly to data while maintaining high-confidence safety for locomotion.

III. Preliminaries

A. Gaussian Processes

To map terrain elevation with uncertainty for bipedal navigation, we employ GP regression:

Definition 1 (Gaussian Process Regression): A GP models a function $g(\boldsymbol{\xi}) \sim \mathcal{N}(\mu(\boldsymbol{\xi}), \kappa(\boldsymbol{\xi}, \boldsymbol{\xi}))$ with mean $\mu : \mathbb{R}^n \to \mathbb{R}^n$ and covariance $\kappa : \mathbb{R}^n \times \mathbb{R}^n \to \mathbb{S}^n_+$. Given m samples $D = \{(\boldsymbol{\xi}^{(\mathrm{i})}, \boldsymbol{z}^{(\mathrm{i})})\}_{i=1}^m$, where $\boldsymbol{\xi}^{(\mathrm{i})} \in \mathbb{R}^n$ is the input (a terrain location $\boldsymbol{\xi}^{(\mathrm{i})} = [x^{(\mathrm{i})}, y^{(\mathrm{i})}]$ in the global frame) and $\boldsymbol{z}^{(\mathrm{i})}$ the elevation observed with Gaussian noise variance σ_ν^2, let $K \in \mathbb{R}^{m\times m}$ be the covariance matrix with $K_{ij} = \kappa(\boldsymbol{\xi}^{(\mathrm{i})}, \boldsymbol{\xi}^{(\mathrm{j})})$. For a test point $\boldsymbol{\xi}'$, define $k(\boldsymbol{\xi}') = [\kappa(\boldsymbol{\xi}', \boldsymbol{\xi}^1)\ \kappa(\boldsymbol{\xi}', \boldsymbol{\xi}^2)\ \ldots\ \kappa(\boldsymbol{\xi}', \boldsymbol{\xi}^m)]^T \in \mathbb{R}^m$. The predictive distribution of g at $\boldsymbol{\xi}'$ is Gaussian with mean and variance

$$\mu_{g|D}(\boldsymbol{\xi}') = k(\boldsymbol{\xi}')^T (K + \sigma_\nu^2 I_m)^{-1} Z, \tag{1a}$$

$$\sigma^2_{g|D}(\boldsymbol{\xi}') = \kappa(\boldsymbol{\xi}', \boldsymbol{\xi}') - k(\boldsymbol{\xi}')^T (K + \sigma_\nu^2 I_m)^{-1} k(\boldsymbol{\xi}'), \tag{1b}$$

where I_m is the identity and $Z = [z^1, \ldots, z^m]^T$.

1) Attentive Kernel: We use the Attentive Kernel (AK) [19] for terrain elevation estimation. The AK adapts to spatial variability through a neural network combining multiple radial basis function (RBF) kernels, with a secondary network assigning membership vectors to decouple nearby correlations. In contrast, the stationary RBF kernel yields uniformly smooth predictions $\kappa^{\mathrm{RBF}}(\boldsymbol{\xi}^{(\mathrm{i})}, \boldsymbol{\xi}^{(\mathrm{j})}) = \sigma_f^2 \exp(-\|\boldsymbol{\xi}^{(\mathrm{i})} - \boldsymbol{\xi}^{(\mathrm{j})}\|^2/2\ell^2)$, with variance σ_f^2 and length-scale ℓ. The AK is defined as

$$\kappa^{\mathrm{AK}}(\boldsymbol{\xi}^{(\mathrm{i})}, \boldsymbol{\xi}^{(\mathrm{j})}) = \alpha \bar{z}^T \bar{z}' + \textstyle\sum_{m=1}^M \bar{w}_m \kappa_m^{\mathrm{RBF}}(\boldsymbol{\xi}^{(\mathrm{i})}, \boldsymbol{\xi}^{(\mathrm{j})}) \bar{w}'_m,$$

where α is a coefficient, $\bar{w}$ and $\bar{z}$ are learned weight and membership vectors, and $\{\kappa_m^{\mathrm{RBF}}(\boldsymbol{\xi}^{(\mathrm{i})}, \boldsymbol{\xi}^{(\mathrm{j})})\}_{m=1}^M$ are RBF kernels with length-scales $\{\ell_m\}_{m=1}^M$.

B. Robot Model

1) Reduced-order robot dynamics: We first introduce the continuous LIP dynamics in the sagittal direction and in the local frame of the robot's stance foot, which is governed by $\ddot{x}^{\mathrm{loc}} = \omega^2 x^{\mathrm{loc}}$, where $x^{\mathrm{loc}} \in \mathbb{R}$ is the CoM sagittal position in the local frame of current stance foot, $\omega = \sqrt{g/z_{\mathrm{H}}}$ is the asymptotic slope, with the gravitational acceleration g and the CoM height at the apex state z_{H}[1], as seen in Fig. 2(a),

[1] Apex state is the state when the CoM is directly on top of the foot.

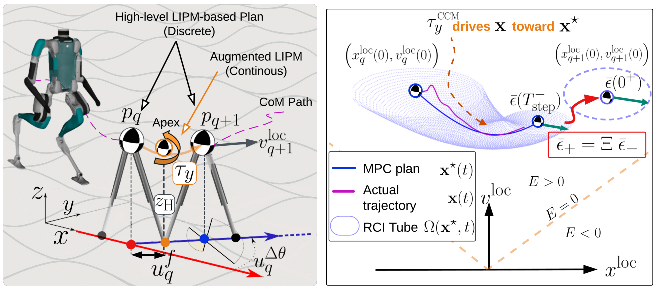

(a) High-level LIPM plan (discrete) (b) Augmented LIPM (continuous)

Fig. 2. (a) The high-level planner's global dynamics is based on the Linear Inverted Pendulum Model (LIPM). For contraction analysis at the low-level, we use the Augmented LIP Model (Aug-LIPM) with flywheel torque τ_y about the CoM. (b) Sagittal phase portrait for one walking step from q^{th} to $(q+1)^{\text{th}}$ in the local frame of the q^{th} footstep. The desired MPC-guided trajectory $\mathbf{x}^\star(t)$ (dark blue) is designed by (2) given the MPC output $(x_q^{\text{loc}}, v_q^{\text{loc}}, u_q^f)$. The true CoM trajectory from full-order dynamics $\mathbf{x}(t)$ (pink) is regulated to track the desired plan via CCM control law τ_y^{CCM}. The RCI tube $\Omega(\mathbf{x}^\star, t)$ (light blue) is constructed around the desired trajectory; orbital energy E is represented by the asymptotic slope line (orange), and tube-bound propagation is shown via the saltation matrix Ξ.

which is constant for all walking steps (i.e., the CoM surface plane is compliant with the terrain shape [9]). Given the local frame of the stance foot, where the distance to the CoM position is denoted by $-u^f$ in the sagittal direction, the closed-form evolution of the sagittal dynamics can be expressed as

$$x^{\text{loc}}(t) = x^{\text{loc}}(0) + \frac{\sinh(\omega t)}{\omega}\, v^{\text{loc}}(0) + \big(1 - \cosh(\omega t)\big) u^f, \tag{2a}$$

$$v^{\text{loc}}(t) = \cosh(\omega t)\, v^{\text{loc}}(0) - \omega \sinh(\omega t)\, u^f. \tag{2b}$$

For high-level locomotion planning, we time-discretize the LIP model with each discrete state defined at the foot-switching instant. By fixing constant the step duration T_{step} in (2), the state at the $(q+1)^{\text{th}}$ step is $x_{q+1}^{\text{loc}} \doteq x_q^{\text{loc}}(T_{\text{step}})$, where $x_q^{\text{loc}}(T_{\text{step}})$ is the state of the continuous dynamics (2a) evaluated at time instant T_{step}. leading to the discrete sagittal LIP local dynamics:

$$x_{q+1}^{\text{loc}} = x_q^{\text{loc}} + \frac{\sinh(\omega T_{\text{step}})}{\omega}\, v_q^{\text{loc}} + \big(1 - \cosh(\omega T_{\text{step}})\big) u_q^f, \tag{3a}$$

$$v_{q+1}^{\text{loc}} = \cosh(\omega T_{\text{step}})\, v_q^{\text{loc}} - \omega \sinh(\omega T_{\text{step}})\, u_q^f. \tag{3b}$$

Following the formulation in [20], the bipedal global state at timestep q is defined as $\mathbf{x}_q = (p_q, v_q^{\text{loc}}, \theta_q) \in \mathbb{R}^5$, where $p_q = (x_q, y_q, z_q)$ is the CoM position in the global frame, v_q^{loc} is the local sagittal velocity, and θ_q is the global heading angle. The control variables are $\mathbf{u}_q = (u_q^f, u_q^{\Delta\theta}) \in \mathbb{R}^2$, where u_q^f is the sagittal foot position relative to the CoM, and $u_q^{\Delta\theta}$ is the global heading change between two consecutive steps, as shown in Fig. 2(a). Applying a coordinate transformation with respect to θ_q to (3a), (3a) yields the 3-D LIP dynamics in the global coordinates (derivations in [20]):

$$x_{q+1} = x_q + \Delta x^{\text{loc}} \cos(\theta_q), \tag{4a}$$

$$y_{q+1} = y_q + \Delta x^{\text{loc}} \sin(\theta_q), \tag{4b}$$

$$z_{q+1} = z_q + \nabla_{x,y}\mu_{g|D}(x_q, y_q)\Delta x^{\text{loc}}, \tag{4c}$$

$$v_{q+1}^{\text{loc}} = \cosh(\omega T) v_q^{\text{loc}} - \omega \sinh(\omega T) u_q^f, \tag{4d}$$

$$\theta_{q+1} = \theta_q + u_q^{\Delta\theta}, \tag{4e}$$

where $\Delta x^{\text{loc}} = x_{q+1}^{\text{loc}} - x_q^{\text{loc}}$ is derived from (3a). The heading update is given by $u_q^{\Delta\theta} = \theta_{q+1} - \theta_q$ and $\nabla_{x,y}\, \mu_{g|D}(x_q, y_q)$ is the estimated slope of the GP terrain map [5]. For compactness, system (4) is denoted as $\mathbf{x}_{q+1} = \Phi(\mathbf{x}_q, \mathbf{u}_q)$.

2) Augmented LIP dynamics: For contraction analysis, we employ an Augmented LIP Model (Aug-LIPM) with the addition of flywheel torque control about the local pitch angle τ_y and bounded disturbance input w, which is governed by

$$\ddot{x}^{\text{loc}} = \omega^2 x^{\text{loc}} - \frac{\omega^2}{mg}\tau_y + w, \tag{5}$$

for a bipedal robot with mass m. We assume $w \in \mathcal{W} \subseteq \mathbb{R}$, where $\mathcal{W}$ is a compact set. We provide the state-space form of the Aug-LIP for the ease of notation interchange in contraction analysis (Sec. III-D) as:

$$\underbrace{\begin{bmatrix} \dot{x}^{\text{loc}} \\ \dot{v}^{\text{loc}} \end{bmatrix}}_{\dot{\mathbf{x}}^{\text{loc}}} = \underbrace{\begin{bmatrix} 0 & 1 \\ \omega^2 & 0 \end{bmatrix}}_{A} \underbrace{\begin{bmatrix} x^{\text{loc}} \\ v^{\text{loc}} \end{bmatrix}}_{\mathbf{x}^{\text{loc}}} + \underbrace{\begin{bmatrix} 0 \\ -\frac{\omega^2}{mg} \end{bmatrix}}_{B} \underbrace{\tau_y}_{\mathbf{u}^{\text{loc}}} + \underbrace{\begin{bmatrix} 0 \\ 1 \end{bmatrix}}_{B_w} w. \tag{6}$$

C. Conformal Prediction

Consider a collection of $k+1$ random variables $R^{(0)}, \dots, R^{(k)}$ that are *exchangeable*[2]. These variables, referred to as *nonconformity scores*, quantify the deviation between predictions and observations. In supervised learning, a common score is $R^{(\mathrm{i})} = R(\boldsymbol{\xi}^{(\mathrm{i})}, \boldsymbol{z}^{(\mathrm{i})}|D) = |\boldsymbol{z}^{(\mathrm{i})} - \mu_D(\boldsymbol{\xi}^{(\mathrm{i})})|$, where $\mu_D(\cdot)$ is a predictive model trained on dataset D to estimate the observation $\boldsymbol{z}^{(\mathrm{i})}$ from input $\boldsymbol{\xi}^{(\mathrm{i})}$. Larger scores correspond to poorer predictive accuracy. The aim of CP is to bound the nonconformity score of a query point $R^{(0)} = |\boldsymbol{z}'_{\text{true}} - \mu_D(\boldsymbol{\xi}')|$ with high probability. For failure rate $\delta \in (0,1)$, we seek a threshold $\mathcal{C}$ such that $P(R^{(0)} \le \mathcal{C}) \ge 1 - \delta$.

A quantile-based approach [21, Lemma 1] constructs $\mathcal{C}$ as the $(1-\delta)$-quantile of the empirical distribution of $\{R^{(1)}, \dots, R^{(k)}\} \cup \{\infty\}$ sorted in non-decreasing order. With this approach, we can define the threshold $\mathcal{C} = R^{(p)}$ where $p = \lceil (k+1)(1-\delta) \rceil$, where $\lceil \cdot \rceil$ is the ceiling function.

Definition 2 (Split Conformal Prediction): Split CP provides computational efficiency by partitioning the dataset $D = D^{\text{train}} \cup D^{\text{cal}}$ into disjoint training and calibration sets. The predictor $\mu(\cdot)$ is fitted on D^{train}, and nonconformity scores $R^{(\mathrm{i})}$ are computed on $(\boldsymbol{\xi}^{(\mathrm{i})}, \boldsymbol{z}^{(\mathrm{i})}) \in D^{\text{cal}}$ for $i = 1, \dots, k$ with $k = |D^{\text{cal}}|$. For a query point $\boldsymbol{\xi}'$ with unknown truth value $\boldsymbol{z}^{\text{true}}$, the prediction interval I_δ is given by:

$$I_\delta(\boldsymbol{\xi}') = \{\boldsymbol{z} \in \mathbb{R} : R(\boldsymbol{\xi}', \boldsymbol{z}\, |D^{\text{train}}) \le \mathcal{C}\}, \tag{7}$$

where $\mathcal{C} = R^{(p)}$ and failure rate δ is user-defined. Under exchangeability of the data, the coverage interval (7) ensures $\mathbb{P}(\boldsymbol{z}^{\text{true}} \in I_\delta(\boldsymbol{\xi}')) \ge 1 - \delta$, or equivalently,

$$\mathbb{P}(\boldsymbol{z}^{\text{true}} \in [\mu_{D^{\text{train}}}(\boldsymbol{\xi}') - \mathcal{C}, \mu_{D^{\text{train}}}(\boldsymbol{\xi}') + \mathcal{C}]) \ge 1 - \delta. \tag{8}$$

[2]Exchangeability means that the joint distribution of $R^{(0)}, \dots, R^{(k)}$ is invariant under any permutation σ of the indices $\{0, \dots, k\}$. It is a weaker assumption than independence and identical distribution (i.i.d.).

D. Control Contraction Metrics

Contraction theory studies incremental stability by examining differential dynamics between neighboring trajectories. In this work, we use control contraction metrics (CCMs) to stabilize our reduced-order model [22]. For simplicity, all discussion in this section is presented in the local frame of the current foot stance, and the superscript $^{\text{loc}}$ is omitted. Given a linear time-invariant system of form (6) with state and control $\mathbf{x} \in \mathbb{R}^{n_x}$, $\mathbf{u} \in \mathbb{R}^{n_u}$ under disturbance $\mathbf{w} \in \mathbb{R}^{n_w}$, a CCM defines a state-feedback tracking control law that ensures that any *disturbance-free* system trajectory $\mathbf{x}(t)$ converges toward a desired *disturbance-free* reference trajectory $\{\mathbf{x}^\star(t), \mathbf{u}^\star(t)\}_{t\geq 0}$ exponentially quickly, i.e., for any $\mathbf{x}(0)$, $\lim_{t\to\infty} \|\mathbf{x}(t) - \mathbf{x}^\star(t)\|_2 = 0$, there exists constants $\Lambda, \lambda > 0$ such that $\|\mathbf{x}(t) - \mathbf{x}^\star(t)\|_2 \leq \Lambda e^{-\lambda t}\|\mathbf{x}(0) - \mathbf{x}^\star(0)\|_2$. The decay rate λ is called the *contraction rate*. Specifically, for LTI systems, a CCM $M \in \mathbb{S}_+^{n_x}$ satisfies the following condition

$$A^\top M + MA - MBB^\top M \preceq -2\lambda M. \tag{9}$$

The resulting feedback law $\mathbf{u}(t) = -\frac{1}{2}\rho B^\top M(\mathbf{x}(t) - \mathbf{x}^*(t))$ renders the noise-free, closed-loop system incrementally exponentially stable, converging to $\mathbf{x}^*(t)$ with contraction rate $\lambda > 0$. While (9) is non-convex, it can be reformulated via variable transformation into a convex semidefinite program (SDP), which can be efficiently solved [11].

1) CCMs, Riemannian Energy, and Invariant Tubes: In the presence of bounded disturbance $\mathcal{W} = \{w \mid \|w\|_2 \leq \bar{w}\}$, instead of ensuring exponential convergence to the reference, the CCM-based controller can ensure that the closed-loop system remains within a robust control invariant tube. To set the stage, we define the Riemannian energy $\mathcal{E}(\mathbf{x}, \mathbf{x}^\star) = (\mathbf{x}(t) - \mathbf{x}^\star(t))^\top M(\mathbf{x}(t) - \mathbf{x}^\star(t))$. From [12], we have

$$\mathcal{E}(\mathbf{x}^\star(t), \mathbf{x}(t)) \leq \left[\sqrt{\mathcal{E}(\mathbf{x}^\star(0), \mathbf{x}(0))}\, e^{-\lambda t} + \bar{d}(1 - e^{-\lambda t})\right]^2. \tag{10}$$

where $\bar{d} = \sigma(M^{\frac{1}{2}}B_w)\bar{w}/\lambda$, where σ is the singular value.

Definition 3 (Robust Control Invariant Tube): A robust control invariant (RCI) tube [12], [13], [23]

$$\Omega(\mathbf{x}^\star, t) := \{\mathbf{x} \in \mathcal{X} : \|\mathbf{x}(t) - \mathbf{x}^\star(t)\|_2 \leq \bar{\epsilon}(t), \forall t \in [0, T_{\text{step}}]\} \tag{11}$$

is defined such that any state starting inside $\Omega(\mathbf{x}^\star, t)$ is guaranteed to remain inside it throughout one walking step of duration T_{step}. Assuming the system (6) with $\|w\|_2 \leq \bar{w}$, we construct a time-varying ellipsoid centered around the reference state $\mathbf{x}^\star(t)$. The maximum radial distance $\bar{\epsilon}(t)$ under $\bar{w}$ which preserves contracting behavior is given by:

$$\bar{\epsilon}(t) = \sqrt{\left(\int_0^t \bar{\mathcal{E}}(t)\, dt\right) \frac{1}{\sqrt{\underline{\lambda}(M)}}},$$

where $\bar{\mathcal{E}}(t)$ is the right-hand side of (10), and $\underline{\lambda}(M)$ is the minimum eigenvalue of M.

2) Saltation Matrix: The saltation matrix Ξ is a first-order approximation of a system's sensitivity to discrete events [24], used to correctly propagate the variation about the nominal trajectory $\delta x(t)$ when a hybrid jump occurs such that $\delta x(t^+) = \Xi \delta x(t^-)$, where $\delta x(t^-), \delta x(t^+)$ denotes the

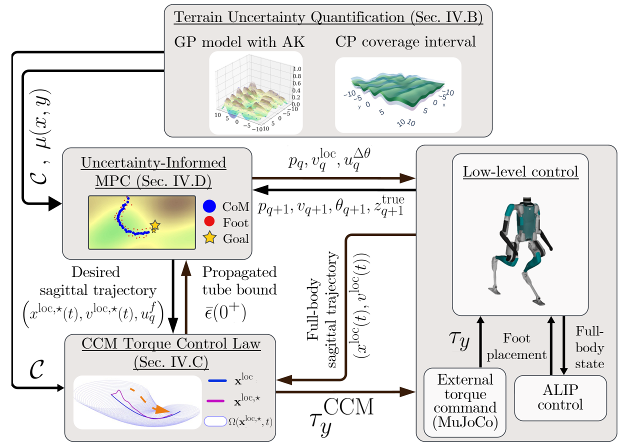

Fig. 3. Overall block diagram of the proposed probabilistically-safe planning and control strategy for bipedal navigation over uncertain terrain.

pre-transition and post-transition, respectively. The dynamics model of a bipedal robot is hybrid, consisting of continuous single-contact dynamics described by (6) (i.e., walking on one stance leg) and discrete double-contact transition (i.e, at the leg switching instance) with assumed duration T_{switch}, for which we define the *guard condition* g and *reset map* $\Delta : \mathbf{x}_- \to \mathbf{x}_+$ as:

$$g : x^{\text{loc}}(0^+) = \tilde{x}^{\text{loc}}(T_{\text{step}}^-),$$

$$\Delta : \begin{cases} x^{\text{loc}}(0^+) & = x^{\text{loc}}(T_{\text{step}}^-) + v^{\text{loc}}(T_{\text{step}}^-) \cdot T_{\text{switch}} - u^f, \\ v^{\text{loc}}(0^+) & = v^{\text{loc}}(T_{\text{step}}^-), \end{cases}$$

where $\tilde{x}^{\text{loc}}(T_{\text{step}}^-)$ is predicted using (2a) given $(x^{\text{loc}}(0^-), v^{\text{loc}}(0^-), u^f)$. Since the RCI tube in Def. 3 relies on continuous propagation of (10), we adopt the saltation matrix Ξ to formally define how the tube bound changes over the discrete transition, which is defined as

$$\Xi = J_\Delta + \frac{(\mathcal{F}^+ - J_\Delta \mathcal{F}^-)J_g^\top}{J_g^\top \mathcal{F}^-},$$

where J_Δ and J_g are the Jacobian matrix of Δ and g evaluated at $\mathbf{x}_-$, respectively, and $\mathcal{F}^\pm = [v^{\text{loc}}(t), \omega^2 x^{\text{loc}}(t)]^\top$ represents the vector field evaluated at state $\mathbf{x}_\pm$.

IV. Methods

A. Framework Overview

We propose a framework for bipedal navigation over rough terrain with elevation uncertainty. From sparse elevation data, the terrain is estimated using a GP model $\mu_{g|D}(\boldsymbol{\xi})$ and combined with CP to obtain coverage intervals I_δ of the true height map (Sec. IV-B). A high-level MPC planner then generates CoM trajectories and footstep sequences with probabilistic safety guarantees (Sec. IV-D). CP-based uncertainty quantification defines contraction-based reachable tubes $\Omega(\mathbf{x}^{\text{loc},\star}, t)$ around the MPC plans (Sec. IV-C.2), while a contraction-based flywheel torque controller stabilizes off-nominal centroidal angular momentum from terrain uncertainty (Sec. IV-C.4). The overall method is shown in Fig. 3.

B. Uncertainty Quantification for Bipedal Footstep Planning

1) Split CP with GP model: We apply Split CP to the GP mean terrain estimate to construct coverage intervals with predefined probability. Unlike GP confidence intervals, which become overly conservative in sparse data due to large variance, Split CP uses the empirical error distribution $R^{(i)}$ to determine a threshold $\mathcal{C}$, yielding tighter intervals of the form $I_\delta = [\mu_{g|D^{\text{train}}}(x,y)-\mathcal{C},\ \mu_{g|D^{\text{train}}}(x,y)+\mathcal{C}]$, as validated in Sec. V. For brevity, we denote $\mu(\cdot)$ as the GP terrain model trained on the split dataset for the remainder of this paper.

2) CP safe footstep constraint: We derive the safety constraint for terrain elevation change between two adjacent footsteps defined by (x_q, y_q, z_q) and $(x_{q+1}, y_{q+1}, z_{q+1})$. We define an inequality $c(z_q, z_{q+1}) \geq 0$ to bound the height change by the maximum feasible limit $\Delta h_{\max}$, where

$$c(z_q, z_{q+1}) = \Delta h_{\max} - |z_{q+1} - z_q|. \tag{12}$$

At each iteration of high-level planning, we assume $z_q = z_q^{\text{true}}$ to be known (i.e., the current foot height can be measured) and assume mean height, $z'_{q+i} = \mu(x_{q+1}, y_{q+1})$, for all future footsteps for $i \in \{1, \ldots, H-1\}$ over the horizon H. We now prove that enforcing (12) ensures a feasible step with probability at least $1-\delta$ despite terrain uncertainty.

Lemma 1 (CP Safe Footstep Constraint): Let $c : \mathbb{R}^n \times \mathbb{R}^n \to \mathbb{R}$ be a Lipschitz continuous function in its second argument with Lipschitz constant $L > 0$, i.e., $|c(\cdot, a) - c(\cdot, b)| \leq L\|a-b\|$ for all a, b. Let $\mathcal{C}$ denote the $(1-\delta)$-quantile of the empirical distribution of random variables $R^{(1)}, \ldots, R^{(k)}$. If the constraint

$$c(z_q, z'_{q+1}) \ \geq\ L\mathcal{C} \tag{13}$$

is enforced at step q, then the true terrain height change between z_q^{true} and z_{q+1}^{true} remains below the feasible limit $\Delta h_{\max}$ with probability at least $1-\delta$.

Proof: At the q^{th} step we have $c(z_q^{\text{true}}, z'_{q+1}) \geq L\mathcal{C}$, since at the first timestep, $z_q = z_q^{\text{true}}$. Since $c(\cdot,\cdot)$ is L-Lipschitz in its second argument, we have

$$c(z_q^{\text{true}}, z_{q+1}^{\text{true}}) \ \geq\ c(z_q^{\text{true}}, z'_{q+1}) - L\left\|z_{q+1}^{\text{true}} - z'_{q+1}\right\|. \tag{14}$$

Substituting the constraint into (14) yields

$$c(z_q^{\text{true}}, z_{q+1}^{\text{true}}) \ \geq\ L(\mathcal{C} - \left\|z_{q+1}^{\text{true}} - z'_{q+1}\right\|). \tag{15}$$

Define the random variable $R = \left\|z_{q+1}^{\text{true}} - z'_{q+1}\right\|$. By the definition of $\mathcal{C}$, $\mathbb{P}(\mathcal{C} - R \geq 0) \ \geq\ 1-\delta$. Thus, the right-hand side of (15) is nonnegative with probability at least $1-\delta$. Consequently, $\mathbb{P}\Big(c(z_q^{\text{true}}, z_{q+1}^{\text{true}}) \ \geq\ 0\Big) \ \geq\ 1-\delta$, which guarantees that the true terrain elevation change at step q satisfies the feasible limit with confidence level $1-\delta$. ■

C. RCI Tube for Phase Space Planning

1) Disturbance bounds for Augmented LIP Model: Given an estimated height $\mu(x_q, y_q)$ at the current stance foot of the q^{th} step and a threshold $\mathcal{C}$, the true terrain height at the q^{th} step, denoted as $\boldsymbol{z}_q^{\text{true}}$, lies in the interval $\boldsymbol{z}_q^{\text{true}} \in I_\delta^q$ with a confidence level of $(1-\delta)$. The Aug-LIPM dynamics (6) are propagated under the assumption that $\omega^2 = \frac{g}{z_H}$, which remains constant due to the assumption of a fixed apex height z_H. This corresponds to constraining the CoM motion to a surface plane parallel to the terrain profile [9]. We account for uncertainty in $\boldsymbol{z}_q^{\text{true}}$ by propagating it to the asymptotic slope, which arises when the true terrain height deviates from the estimated height used in the Aug-LIPM. Specifically, instead of assuming a fixed z_H, we have $\omega_{\text{true}}^2 \in [\frac{g}{(z_H+\mathcal{C})}, \frac{g}{(z_H-\mathcal{C})}] \doteq \omega^2 + C_\Delta$, where $C_\Delta \in [\frac{-g\mathcal{C}}{z_{\mathrm{H}}(z_{\mathrm{H}}+\mathcal{C})}, \frac{g\mathcal{C}}{z_{\mathrm{H}}(z_{\mathrm{H}}-\mathcal{C})}]$. Thus, the Aug-LIPM in (5) becomes

$$\ddot{x}^{\text{loc}} = \omega^2 x^{\text{loc}} - \frac{\omega^2}{mg}\tau_y + w_{\text{terrain}}, \tag{16}$$

where $w_{\text{terrain}} = C_\Delta(x^{\text{loc}} - \frac{\tau_y}{mg})$, and $x^{\text{loc}} \in \mathcal{X}^{\text{loc}} \doteq [x_{\min}^{\text{loc}}, x_{\max}^{\text{loc}}]$ and $\tau_y \in \mathcal{U}^{\text{loc}} \doteq [\tau_{y,\min}, \tau_{y,\max}]$ are bounded by feasible state and control constraints. We then define a terrain-uncertainty related bounded set of disturbances w in (6) as $\mathcal{W}_{\text{terrain}} \doteq \{w : \|w\| \leq \bar{w}_{\text{terrain}}\}$, where we use the upper bound $\bar{w}_{\text{terrain}} = \max_{\{x\in\mathcal{X}^{\text{loc}}, \tau\in\mathcal{U}^{\text{loc}}\}} |C_\Delta||x - \frac{\tau}{mg}|$.

2) RCI tube for sagittal phase-space dynamics: We define the reference trajectory for the Aug-LIPM $\{\mathbf{x}^{\text{loc},\star}(t)\, \mathbf{u}^{\text{loc},\star}(t)\}$ as sagittal trajectory guided by (2) given high-level planner's output $(x_q^{\text{loc}}, v_q^{\text{loc}}, u_q^f)$ (i.e., $\mathbf{u}^{\text{loc},\star} = \tau_y^\star = 0$. Given the sytem (6) is a linear time-invariant with control matrix B, the CCM M in (9) provides the flywheel torque control law that exponentially stabilizes the true trajectory toward $\mathbf{x}^{\text{loc},\star}(t)$

$$\tau_y^{\text{CCM}}(t) = -\frac{1}{2}\rho B^\top M(\mathbf{x}^{\text{loc}}(t) - \mathbf{x}^{\text{loc},\star}(t)). \tag{17}$$

Remark 1: CoM sagittal states $\mathbf{x}^{\text{loc}}$ governed by (6) that are initialized in the RCI tube (11) are guaranteed to stay within the tube for all $t \in [0, T_{\text{step}}]$ under the CCM control law τ_y^{CCM}, which ensure forward invariance around the desired motion plans $\{\mathbf{x}^{\text{loc},\star}, \mathbf{u}^{\text{loc},\star}\}$. We also emphasize that exiting the RCI tube does not imply a fall; it only implies that forward invariance in (11) is not guaranteed; in practice, (17) can still effectively compensate for terrain-uncertainty-induced perturbations w_{terrain}.

3) Saltation matrix tube propagation: During the discrete transition, corresponding to the foot-switching instant between walking steps, we propose a formal propagation rule for the upper bound of the Riemannian energy across the transition using the saltation matrix. The propagation is given by: $\bar{\mathcal{E}}^+(0) = \boldsymbol{\epsilon}^\top \Xi^\top M \Xi \boldsymbol{\epsilon}$, where $\boldsymbol{\epsilon} \in \mathbb{R}^2$ is any vector of norm $\|\boldsymbol{\epsilon}\|_2 = \bar{\epsilon}_-(T_{\text{step}})$, which is the RCI tube bound at the end of the step. By the construction of our guard condition and reset map in Def. III-D.2, the determinant $\|\Xi\| > 1$ implies that Ξ is expansive. Given this result, we prove that the sagittal state of the robot is guaranteed to remain forward invariant over a single step with probability at least $1-\delta$ (Lem. 2) and over i steps with probability at least $(1-\delta)^i$ (Lem. 3).

Lemma 2: Given terrain coverage interval with confidence level $1-\delta$, the sagittal state governed by (6) initialized inside the RCI tube $\Omega(\mathbf{x}^{\text{loc},\star}, t)$ is guaranteed to stay within the tube under the CCM control law $\tau_y^{\text{CCM}}(t)$ (17) for all $t \in [0, T_{\text{step}}]$ during *one* walking step under any disturbance in terrain height with probability $1-\delta$.

Proof: Following (3), the RCI tube $\Omega(\mathbf{x}^{\text{loc},\star}, t)$ satisfies an upper-bound $\bar{\epsilon}(t)$ determined by $\bar{w}_{\text{terrain}}$ such that $\|\mathbf{x}^{\text{loc}}(t) - \mathbf{x}^{\text{loc},\star}(t)\| \leq \bar{\epsilon}(t), \forall t \in [0, T_{\text{step}}]$. From the CP coverage guarantees, we have that $w \in \mathcal{W}_{\text{terrain}}$, i.e., the disturbance bound is valid, with probability at least $1-\delta$. Thus, $\mathbf{x}^{\text{loc}}(t) \in \Omega(\mathbf{x}^{\text{loc},\star}, t)$ with probability at least $1-\delta$. ■

Lemma 3: Over i walking steps, the probability of the terrain-perturbed dynamics (16) staying in the RCI tube for $i \in \{1, \dots, H-1\}$ is at least $(1+\delta)^i$, where H is the horizon.

Proof: Lem. 2 guarantees RCI tube invariance with probability $(1-\delta)$ for the sagittal CoM states such that $\mathbf{x}^{\text{loc}}(t) \in \Omega(\mathbf{x}^\star, t) \iff \|\mathbf{x}^{\text{loc}}(t) - \mathbf{x}^{\text{loc},\star}(t)\|_2 \leq \bar{\epsilon}(t)$ for all $t \in [0, T_{\text{step}}]$. During the discrete transition, the state variation at the end of the step, $\delta x(T_{\text{step}}^-) \doteq \mathbf{x}^{\text{loc}}(T_{\text{step}}^-) - \mathbf{x}^{\text{loc},\star}(T_{\text{step}}^-)$, and the RCI tube bound $\bar{\epsilon}(T_{\text{step}}^-)$ are both propagated by the saltation matrix as follows:

$$\delta x(0^+) = \Xi\, \delta x(T_{\text{step}}^-), \quad \bar{\epsilon}(0^+) = \Xi\, \bar{\epsilon}(T_{\text{step}}^-).$$

If $\mathbf{x}^{\text{loc}}(T_{\text{step}}^-) \in \Omega(\mathbf{x}^{\text{loc},\star}, T_{\text{step}}^-)$ during the current walking step, then $\|\delta x(T_{\text{step}}^-)\| \leq \bar{\epsilon}(T_{\text{step}}^-)$. Since the saltation matrix is expansive with $\|\Xi\| \geq 1$, we guarantee that the bound in the next walking step satisfies

$$\Xi\|\delta x(T_{\text{step}}^-)\| \leq \Xi\bar{\epsilon}(T_{\text{step}}^-) \to \|\delta x(0^+)\| \leq \bar{\epsilon}(0^+). \tag{18}$$

Therefore, $\mathbf{x}^{\text{loc}}(0^+) \in \Omega(\mathbf{x}^{\text{loc},\star}, 0^+)$ holds for the next walking step. Since $\mathbf{x}^{\text{loc}}(0^+)$ is initialized inside the RCI tube, Lem. 2 ensures that it will remain invariant within the tube for the remainder of the step under bounded disturbance set $\mathcal{W}_{\text{terrain}}$ with probability of $(1-\delta)$. For i number of walking steps, where each step is an independent event since the true foot height is re-measured after the step, the tube invariance probability compounds according to the product rule, $\mathbb{P}\Big(\bigcup_i \big(\, \mathbf{x}_i^{\text{loc}}(t) \in \Omega(\mathbf{x}_i^{\text{loc},\star}, t); \forall t \in [0, T_{\text{step}}]\big)\Big) = (1-\delta)^i$ for $i \in [1, ..., H-1]$. ■

4) Contraction-based controller for full-order dynamics: Throughout the paper, the RCI tube $\Omega(\mathbf{x}^{\text{loc},\star}, t)$ and the CCM control law $\tau_y^{\text{CCM}}(t)$ are derived by the Augmented LIP dynamics. Here, we provide a formal proof that the contraction analysis of IV-C can be extended to stabilize the full-order robot dynamics.

To realize full-order dynamics, we employ the ALIP planner[3] [2] to generate desired foot placements, together with a passivity-based controller [25] for the low-level control, which achieves asymptotic tracking at the joint level. Ankle actuation is incorporated within the passivity-based controller to enhance the ROM tracking performance [26]. To this end, we implement CCM control law as an flywheel torque applied directly at the robot's CoM within the MuJoCo simulation environment [27]. Nonetheless, model mismatch between the ROM-based trajectory and the full-order dynamics persists due to imperfections in low-level control. We therefore state the following assumption regarding the model error.

Assumption 1: Under a low-level controller with sufficiently stable tracking performance, the sagittal dynamics discrepancy w_{model} between the ROM and the full-order model of the bipedal robot is bounded and belongs to $\mathcal{W}_{\text{model}} \doteq \{w_{\text{model}} \mid \|w_{\text{model}}\| \leq \bar{w}_{\text{model}}\}$, as shown in [28]. w_{model} can also be treated as a disturbance in the linear system (6).

Similar to the approximation approach in [28], we estimate the full-order sagittal dynamics using the Aug-LIPM (6):

$$\dot{\mathbf{x}}^{\text{full}} = A\mathbf{x}^{\text{full}} + B\tau_y^{\text{full}} + w_{\text{terrain}} + w_{\text{model}}, \tag{19}$$

where $\mathbf{x}^{\text{full}} = [x^{\text{loc,full}}, v^{\text{loc,full}}]^\top \in \mathbb{R}^2$ is the true sagittal CoM states of the robot, $w_{\text{terrain}} \in \mathcal{W}_{\text{terrain}}$ and $w_{\text{model}} \in \mathcal{W}_{\text{model}}$ is treated as the bounded model discrepencies between ROM and full-order dynamics under Assumption 1.

Without loss of generality, we can set $\mathbf{x}^{\text{loc},\star}$ (the Aug-LIPM reference to be tracked) as $\mathbf{x}^{\text{LIPM}}$, since $\mathbf{u}^{\text{loc},\star} = \tau_y^\star = 0$. We can leverage the CCM torque (17) as the full-order sagittal control input, denoted in a gain matrix form as $\tau_y^{\text{full}} = \tau_y^{\text{CCM}} = K(\mathbf{x}^{\text{full}} - \mathbf{x}^{\text{LIPM}})$, where $K = -\frac{1}{2}\rho B^\top M$. Then, the error between the full-order and ROM-based sagittal trajectory $e \doteq \mathbf{x}^{\text{full}} - \mathbf{x}^{\text{LIPM}}$ evolves under the closed-loop error dynamics: $\dot{e} = (A+BK)e + w_{\text{terrain}} + w_{\text{model}}$.

Since $A+BK$ is exponentially stable via the CCM, the error converges to a disturbance-invariant set Θ: if $e_0 \in \Theta$, then $e(t) \in \Theta$, $\forall t \geq 0$. By Lem. 2–3, the RCI tube ensures that the error between the full-order and ROM-based trajectories caused by w_{terrain} remains in $\Omega(\mathbf{x}^{\text{loc},\star}, t)$ for all $t \geq 0$ and across all steps. Since disturbances in (19) are additive, Assumption 1 guarantees that the error due to w_{model} also remains invariant within $\Omega(\mathbf{x}^{\text{loc},\star}, t)$ by adjusting the bound $\bar{\epsilon}(t)$ with respect to the combined disturbance $\bar{w} = \bar{w}_{\text{terrain}} + \bar{w}_{\text{model}}$.

In this work, we do not account for $\bar{w}_{\text{model}}$ in constructing the RCI tube. While this may slightly degrade tracking performance of the control law (17), we avoid overly conservative bounds so the entire RCI tube lies within the stable region of the phase portrait (Fig. 2(b)). We later enforce a constraint in Sec. IV-D restricting the RCI tube to the stable domain of positive orbital energy. For the bipedal robot, maintaining positive orbital energy ensures the CoM trajectory remains bounded around foot placement rather than diverging, thereby preventing falls.

D. Uncertainty-Informed Model Predictive Control

Given a terrain map estimated by GP mean $\mu(x, y)$ and $\mathcal{C}$, we formulate a high-level planner via MPC with horizon H using global dynamics (4) with state $\mathbf{x} = (x, y, z, v^{\text{loc}}, \theta)$ and control $\mathbf{u} = (u^f, u^{\Delta\theta})$ as follows:

$$\begin{aligned}
\min_{\mathbf{x}_{0:H}, \mathbf{u}_{0:H-1}} \quad & \|p_N - p_{\mathcal{G}}\|_{W_1}^2 + \|\theta_N - \theta_{\mathcal{G}}\|_{W_2}^2 && \text{(20a)}\\
& + \textstyle\sum_{q=0}^{H-1} \|\nabla_{x,y}\ \mu(x_q, y_q)\|_{W_3}^2 && \\
\text{s.t.} \quad & \mathbf{x}_{q+1} = \Phi(\mathbf{x}_q, \boldsymbol{u}_q), \forall q \in [1, H-1] && \text{(20b)}\\
& \mathbf{x}_0 = \mathbf{x}_{\text{init}},\ (\mathbf{x}_q, \boldsymbol{u}_q) \in \mathcal{XU}_q, \forall q && \text{(20c)}\\
& c(z_q, z_{q+1}) \geq L\mathcal{C} && \text{(20d)}\\
& z_0 = \boldsymbol{z}^{\text{true}}, z_q = \mu(x_q, y_q), \forall q && \text{(20e)}\\
& E(x_q^{\text{loc},\star}(s), v_q^{\text{loc},\star}(s), \bar{\epsilon}_q(s)) > 0, && \\
& \qquad \forall s \in [0, T_{\text{step}}], \forall q, && \text{(20f)}
\end{aligned}$$

[3] Since our ROM-based planner and controller are designed based on the sagittal dynamics. The lateral dynamics are considered at the lower level using the Angular Momentum LIP model [2], since these motions are periodic given a fixed desired lateral foot placement.

TABLE I

SIMULATION RESULTS (85% CONFIDENCE LEVEL)

Framework / Terrain	T1	T2	T3
Average Norm Error (across all steps) $\|\mathbf{x}^{\rm loc}(t) - \mathbf{x}^{\rm loc,\star}(t)\|_{\rm AVG}$			
Ours	0.040	0.045	0.039
Ours w/o $\tau_y^\star$	Fail	Fail	0.051
Baseline MPC [5]	Fail	Fail	0.052
Prob. of staying within the RCI Tube $\text{P}(\|\mathbf{x}^{\rm loc}(t) - \mathbf{x}^{\rm loc,\star}(t)\| \leq \bar{\epsilon}(t)\ ;\forall t \in [0, T_{\rm step}])$			
Ours	84.94%	77.09%	77.53%
Ours w/o $\tau_y^\star$	Fails	Fails	58.03 %
Baseline MPC [5]	Fails	Fails	54.75%

'Fail' denotes Digit falls, reaching the goal in fewer than 5 of 15 trajectories.

TABLE II

PERFORMANCE ON TERRAIN T3

Method	Sim Time	# of Steps	CP Coverage
Ours	62.30	142.33	85.85%
Ours w/o $\tau_y^\star$	66.32	149.13	80.69%
Baseline MPC [5]	69.75	154.60	81.62%

TABLE III

SIMULATION RESULTS (99.5% CONFIDENCE LEVEL)

Framework / Terrain	T4	T5
$\|\mathbf{x}^{\rm loc}(t) - \mathbf{x}^{\rm loc,\star}(t)\|_{\rm AVG}$		
Ours	0.031	0.034
Baseline MPC [5]	0.051	0.058
$\text{P}(\|\mathbf{x}^{\rm loc}(t) - \mathbf{x}^{\rm loc,\star}(t)\| \leq \bar{\epsilon}(t)\ ;\forall t \in [0, T_{\rm step}])$		
Ours	93.60%	92.41%
Baseline MPC [5]	65.03%	61.42%

where $\mathcal{XU}_q = \{(\mathbf{x}_q, \boldsymbol{u}_q) \mid \mathbf{x}_{\rm lb} \leq \mathbf{x}_q \leq \mathbf{x}_{\rm ub},\ \boldsymbol{u}_{\rm lb} \leq \boldsymbol{u}_q \leq \boldsymbol{u}_{\rm ub}\}$. The MPC cost is adopted from [5], which penalizes the Euclidean distance between the terminal state (i.e., the final position p_N and the heading θ_N) and the goal (i.e., the goal location $p_{\mathcal{G}}$ and the angle between the current position and the goal $\theta_{\mathcal{G}}$) and accumulates penalties over the norm of the terrain traversal slope $\nabla_{x,y}\ \mu(x_q, y_q)$ to avoid regions with steeper terrain. (20d) represents the CP safe footstep constraint, where $z_0 = \boldsymbol{z}^{\rm true}$ and $z_q = \mu(x_q, y_q), \forall q \in \{1, \ldots, H-1\}$, implying that the true terrain height is known only at the stance foot of the current walking step for every iterations. W_1, W_2, and W_3 are weighting matrices.

Remark 2: From Lem. 1, (20d) ensures safe footstep selection with probability at least $1-\delta$ at the first step, consistent with the receding-horizon MPC. For the next $(q+i)$ steps where $i \in \{1, \ldots, H-1\}$, Lem. 3 ensures a safety probability $\mathbb{P}(c(z_q, z_{q+1}) > 0 \cup \cdots \cup c(z_{q+i}, z_{q+i+1}) > 0) = (1-\delta)^i$, since foot height is re-measured at each step, making safety events independent. The choice of δ for different scenarios is discussed in Sec. V.

The constraint (20f) enforces that the orbital energy E of the continuous sagittal phase-space trajectory during the $q^{\rm th}$ step, $x_q^{\rm loc,\star}(s), v_q^{\rm loc,\star}(s)$ governed by (2) given input u_q^f and initial condition $x_q^{\rm loc}, v_q^{\rm loc}$ given by MPC, together with the RCI tube bounds $\bar{\epsilon}_q(s)$ parameterized by $s \in [0, T_{\rm step}]$, remains positive. Note that $x_q^{\rm loc,\star}(s), v_q^{\rm loc,\star}(s)$ is also the desired reference trajectory in our contraction analysis. As seen in Fig. 2(b), positive orbital energy $E > 0$ ensures the robot's CoM has sufficient forward momentum to escape the gravitational pull of its current stance foot and move onto the next step [7]. Graphically, this ensures that the RCI tube never crosses the asymptotic slope line defined in the phase-space plot. Finally, to enforce (20f) over multiple walking steps within the horizon H, we apply the saltation matrix Ξ to propagate the tube bounds from $\bar{\epsilon}_q(T_{\rm step}^-)$ to $\bar{\epsilon}_{q+1}(0^+)$.

V. RESULTS

We evaluate the framework in MuJoCo simulations of the Digit bipedal robot across three distinct $20\,\text{m} \times 20\,\text{m}$ terrains with height from 0 to 0.7 m, which are T1, T2 and T3 (Fig. 4). Results at the 85% safety level are summarized in Table I, with further analysis of T3 in Table II. We also test smaller $6\,\text{m} \times 6\,\text{m}$ terrains T4 and T5 (height from 0 to 0.2 m), where improved GP accuracy, due to smaller input domain, enables 99.5% confidence guarantees over multiple steps (Table III). Our MPC framework, with and without CCM torque control, is compared against the baseline in [5] with only traversal slope minimalization. For each terrain and framework, 15 trajectories with an average of 140 steps are simulated between pre-defined start and goal positions, using full-order dynamics in MuJoCo.

From 2500 discretized map points, 700 are randomly sampled with a 70-30 split (490 training, 210 calibration). At 85% confidence, the average CP threshold across three terrains is $\mathcal{C}_{\rm AVG} = 0.078$ while the GP bound is 0.360 (i.e., $\pm 1.44\sigma(\boldsymbol{\xi})_{\rm AVG}$), and for 99.5% confidence, $\mathcal{C}_{\rm AVG} = 0.060$ while GP bound is 0.708 (i.e., $\pm 2.81\sigma(\boldsymbol{\xi})_{\rm AVG}$). Thus, GP model coupled with CP method yields less conservative bounds, while preserving high confidence level. Table I reports the average norm error (ANE) between $\mathbf{x}^{\rm loc}(t)$ and $\mathbf{x}^{\rm loc,\star}(t)$, measured at 200 Hz across trials, along with the probability of RCI tube invariance, computed as $(\sum_{q=0}^{N} \mathbb{1}^q_{\Omega-\text{invariance}})/N$, where $\mathbb{1}^q_{\Omega\text{-invariance}} = 1$ if $\|\mathbf{x}^{\rm loc}(t) - \mathbf{x}^{\rm loc,\star}(t)\| \leq \bar{\epsilon}(t)$ for all $t \in [0, T_{\rm step}]$, and 0 otherwise. Table II further details terrain T3 performance, including average simulation time, total steps, and CP coverage, defined as $(\sum_{q=0}^{N} \mathbb{1}^q_{\text{true coverage}})/N$, with $\mathbb{1}^q_{\text{true coverage}} = 1$ if $\boldsymbol{z}_q^{\rm true} \in [\mu(\boldsymbol{\xi}_q) - \mathcal{C},\ \mu(\boldsymbol{\xi}_q) + \mathcal{C}]$ during the $q^{\rm th}$ step, and 0 otherwise.

On terrains T1 and T2, the robot fails to reach the goal in fewer than 5 of 15 trials when using baseline MPC or omitting the CCM control law $\tau_y^{\rm CCM}$. On rough terrains with small, frequent height changes (T1) and steeper slopes (T2), $\tau_y^{\rm CCM}$ improves stability by correcting off-nominal centroidal angular momentum, whereas the baselines lack recovery from sudden terrain variations and thus fail. On terrain T3, $\tau_y^{\rm CCM}$ reduces ANE relative to the baseline, yielding trajectories that track the MPC plan more closely, enabling more reliable goal reaching in fewer steps.

To validate Lem. 2, we evaluate the probability of remaining within the RCI tube, expected at 85% (i.e., $\mathbf{x}^{\rm loc}(t)$ would exit the tube only if the true terrain lies outside the CP interval). As noted in Sec. IV-C.4, the torque control $\tau_y^{\rm CCM}$ may suffer slight performance loss from model mismatch. On terrain T1, with bumpy ground and minimal sagittal mismatch, $\tau_y^{\rm CCM}$ maintains the CoM within the tube at the target probability. On terrains T2 and T3, where sloped paths amplify sagittal and vertical perturbations, $\tau_y^{\rm CCM}$ still preserves tube invariance under terrain disturbances and mismatch with only an 8% reduction from the desired 85%,

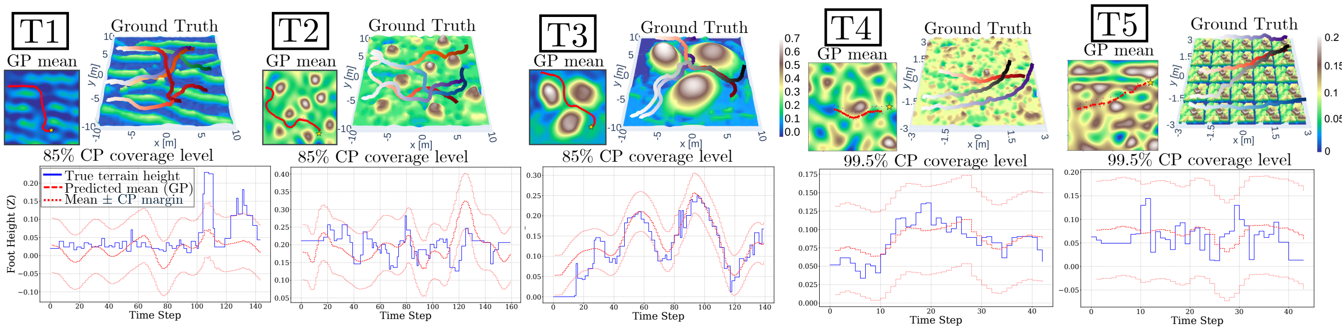

Fig. 4. Visualization of three large terrain profiles, T1: bumpy and rough, T2: wavy and coarse, and T3: hilly with a smoother surface (for the case study with the 85% confidence level), and two smaller terrain profiles, T4 and T4: level but rough (for the case study with the 99.5% confidence level) with sample trajectories from different runs (white indicates the start of each trajectory). For the red trajectory, we show the GP mean estimate map along with the CP confidence interval, which ensures coverage of the true terrain height at each confidence level.

markedly outperforming the baseline or without τ_y^{CCM}.

On terrain T3, both simulation time and step count are reduced compared to the baseline, regardless of whether τ_y^{CCM} is applied. This improvement arises from the CP constraint in (20d), which enables risk-seeking footstep planning by allowing exploration of regions with poor GP elevation estimates, provided true terrain variations lie within CP coverage intervals. Coupled with τ_y^{CCM}, our framework thus yields footstep plans that ensure safe terrain transitions with a level of confidence 85% at every step. Finally, we evaluate our framework on smaller terrains (T4 and T5) at a higher confidence level of 99.5%. By Lem. 3, this guarantees RCI tube invariance for about 20 steps with compounded safety probability $(99.5\%)^{20} \approx 90.5\%$, strongly guaranteeing that the robot will track the full, safe MPC plan. As shown in Table III, our framework achieves over 92% per-step tube invariance and significantly lower ANE than the baseline. Thus, for short-horizon locomotion on immediate terrain with sparse data, GP with CP provides practical probabilistic guarantees for the full trajectory, and when combined with CCM torque control, enables reliable tracking of desired motion plans with high confidence.

VI. Conclusion

We present a planning and control framework for bipedal navigation over uncertain terrain with probabilistic safety guarantees. Two core components of this framework include constructing a contraction-based reachable tube around the CoM trajectory to ensure safe tracking under terrain uncertainty and designing a flywheel torque control law to stabilize CoM angular momentum.

References

[1] A. Torres-Pardo, D. Pinto-Fernández, M. Garabini, F. Angelini, D. Rodriguez-Cianca, S. Massardi, J. Tornero, J. C. Moreno, and D. Torricelli, "Legged locomotion over irregular terrains: State of the art of human and robot performance," *Bioinspiration & Biomimetics*, vol. 17, no. 6, p. 061002, 2022.

[2] G. Gibson, O. Dosunmu-Ogunbi, Y. Gong, and J. Grizzle, "Terrain-adaptive, alip-based bipedal locomotion controller via model predictive control and virtual constraints," in *IROS*, 2022.

[3] J.-K. Huang and J. W. Grizzle, "Efficient anytime clf reactive planning system for a bipedal robot on undulating terrain," *TRO*, 2023.

[4] K. Muenprasitivej, J. Jiang, A. Shamsah, S. Coogan, and Y. Zhao, "Bipedal safe navigation over uncertain rough terrain: Unifying terrain mapping and locomotion stability," in *IROS*, 2024.

[5] A. Shamsah, J. Jiang, Z. Yoon, S. Coogan, and Y. Zhao, "Terrain-aware model predictive control of heterogeneous bipedal and aerial robot coordination for search and rescue tasks," 2024.

[6] S. Kajita, F. Kanehiro, K. Kaneko, K. Yokoi, and H. Hirukawa, "The 3d linear inverted pendulum mode: a simple modeling for a biped walking pattern generation," in *IROS*, 2001.

[7] X. Xiong and A. D. Ames, "Orbit characterization, stabilization and composition on 3d underactuated bipedal walking via hybrid passive linear inverted pendulum model," in *IROS*, 2019.

[8] E. Dantec, W. Jallet, and J. Carpentier, "From centroidal to whole-body models for legged locomotion: a comparative analysis," in *Humanoids*, 2024.

[9] Y. Zhao, B. R. Fernandez, and L. Sentis, "Robust optimal planning and control of non-periodic bipedal locomotion with a centroidal momentum model," *IJRR*, 2017.

[10] W. Lohmiller and J.-J. E. Slotine, "On contraction analysis for non-linear systems," *Automatica*, vol. 34, no. 6, pp. 683–696, 1998.

[11] I. Manchester and J.-J. Slotine, "Control contraction metrics: Convex and intrinsic criteria for nonlinear feedback design," *TAC*, 2017.

[12] S. Singh, B. Landry, A. Majumdar, J.-J. Slotine, and M. Pavone, "Robust feedback motion planning via contraction theory," *IJRR*, 2023.

[13] G. Chou, N. Ozay, and D. Berenson, "Model error propagation via learned contraction metrics for safe feedback motion planning of unknown systems," 2021.

[14] V. Vovk, A. Gammerman, and G. Shafer, *Algorithmic learning in a random world*. Springer Science & Business Media, 2005.

[15] G. Shafer and V. Vovk, "A tutorial on conformal prediction." *Journal of Machine Learning Research*, vol. 9, no. 3, 2008.

[16] L. Lindemann, M. Cleaveland, G. Shim, and G. Pappas, "Safe planning in dynamic environments using conformal prediction," *RA-L*, 2023.

[17] D. Sun, M. J. Khojasteh, S. Shekhar, and C. Fan, "Uncertain-aware safe exploratory planning using gaussian process and neural control contraction metric," in *L4DC*, 2021.

[18] A. Pion and E. Vazquez, "Gaussian process interpolation with conformal prediction: Methods and comparative analysis," in *Machine Learning, Optimization, and Data Science*, 2025.

[19] W. Chen, R. Khardon, and L. Liu, "Ak: Attentive kernel for information gathering," in *Robotics: Science and Systems (RSS)*, 2022.

[20] A. Shamsah, K. Agarwal, N. Katta, A. Raju, S. Kousik, and Y. Zhao, "Socially acceptable bipedal robot navigation via social zonotope network model predictive control," 2024.

[21] R. J. Tibshirani, R. Foygel Barber, E. Candes, and A. Ramdas, "Conformal prediction under covariate shift," *NeurIPS*, 2019.

[22] I. Manchester and J.-J. Slotine, "Control contraction metrics and universal stabilizability," *IFAC*, 2014.

[23] G. Chou, N. Ozay, and D. Berenson, "Safe output feedback motion planning from images via learned perception modules and contraction theory," in *WAFR*, 2022.

[24] N. J. Kong, J. Joe Payne, J. Zhu, and A. M. Johnson, "Saltation matrices: The essential tool for linearizing hybrid dynamical systems," *Proceedings of the IEEE*, vol. 112, no. 6, pp. 585–608, 2024.

[25] H. Sadeghian, C. Ott, G. Garofalo, and G. Cheng, "Passivity-based control of underactuated biped robots within hybrid zero dynamics approach," in *ICRA*, 2017.

[26] A. Shamsah, Z. Gu, J. Warnke, S. Hutchinson, and Y. Zhao, "Integrated task and motion planning for safe legged navigation in partially observable environments," *T-RO*, 2023.

[27] E. Todorov, T. Erez, and Y. Tassa, "Mujoco: A physics engine for model-based control," in *IROS*, 2012.

[28] X. Xiong and A. Ames, "3-d underactuated bipedal walking via h-lip based gait synthesis and stepping stabilization," *TRO*, 2022.